

基于游标效应的并联法布里-珀罗干涉仪传感特性的分析

罗春晖¹, 陈晓旭¹, 吴舜^{1,2*}

¹武汉工程大学光学信息与模式识别湖北省重点实验室, 湖北 武汉 430205;

²中国科学院西安光学精密机械研究所瞬态光学与光子技术国家重点实验室, 陕西 西安 710119

摘要 针对应用高阶谐波游标效应时出现的内包络消失、外包络可见度低等问题,从理论分析和实验探索两方面出发,得出了降低传感腔和参考腔的光强差异可以提高光谱质量的结论。此外,通过合理设计优化传感腔与参考腔的腔长、折射率等影响游标放大倍数的参数,在实验上采用平行结构的法布里-珀罗干涉仪制成了一阶谐波游标效应的光纤气压传感器,不仅获得了高对比度的游标干涉光谱,还在 10~190 kPa 气压范围内,实现了 152 pm/kPa 的气压灵敏度,线性度高达 99%,对应的放大倍数可达到 35.3。

关键词 光纤光学; 光纤传感; 气压传感; 光学游标效应; 游标光谱

中图分类号 TQ342+.82

文献标志码 A

DOI: 10.3788/AOS221550

1 引言

光纤干涉仪型的传感器具有抗电磁干扰、灵敏度高等一系列优点,因而受到了广泛关注^[1-3]。光学游标效应能够增强干涉仪的传感能力,就像游标卡尺能提高测量精度那样^[4],故被广泛应用于温度、气压、应力等诸多光纤传感领域中^[5-19]。理论上,当干涉仪的传感腔和参考腔满足游标条件($n_2L_2 = jn_1L_1 + \Delta L$)时,就可以产生光学游标效应^[20]。其中, $j, \Delta L$ 分别是传感腔与参考腔频率相差的倍数和失谐量, n_1, n_2 和 L_1, L_2 分别表示传感腔与参考腔的折射率和腔长。先前的工作^[20-21]已经表明,游标放大倍数与 j 的数值成正比,与失谐比 $\Delta L / (n_1L_1)$ 成反比,并且在失谐比足够小或者 j 的数值比较大时,传感器的放大倍数可以达到几十^[22-25],甚至上百^[26-27]。虽然光学游标效应有如此优势,但是在涉及高阶谐波游标效应($j > 1$)的应用时,往往会出现随着 j 的增大,外包络的对比度下降、内包络消失等问题,使数据分析变得困难。文献^[21]表明, $j=3$ 时外包络对比度会下降到 0.5 dB 以下,难以用于数据分析。虽然文献^[20]采用提取内包络的方法实现了基本游标效应($j=1$)到三次谐波游标效应($j=4$)的探索,但是该类型传感器采用的设计具有较高的技术难度,难以广泛应用。到目前为止,鲜有关于如何推广高阶谐波游标效应的工作。

本文基于并联式法布里-珀罗干涉仪结构的气压传感器,在实验方面完成了不同阶次的光学游标效应的探索。从实验结果出发,结合理论模拟,找出了应用高阶谐波游标效应时,产生高质量游标光谱(包括清晰内包络)的基本条件,并提出了在气压传感中应用光学游标效应时获得更高放大倍数的普适性方法。本研究对高阶谐波游标效应的广泛应用和高灵敏度的传感器设计都具有一定的借鉴作用。

2 基本原理

本工作采用两个平行的法布里-珀罗干涉仪的结构来充当并联式气压传感器的两条臂,如图 1 所示。由于耦合器到反射镜 M_1, M_2 的长度近似相等,故 4 个反射面 $M_i (i=1, 2, 3, 4)$ 产生的反射电场可以表示为

$$E_r = E_0 \left[\sqrt{R_1} + \sqrt{R_3} + (1 - \alpha_1)(1 - R_1) \sqrt{R_2} \times \exp(-j\phi_1) + (1 - \alpha_2)(1 - R_3) \sqrt{R_4} \exp(-j\phi_2) \right], \quad (1)$$

式中: $\phi_1 = 4\pi n_1 L_1 / \lambda - \pi$, 其中 λ 为波长; $\phi_2 = 4\pi n_2 L_2 / \lambda - \pi$; E_0 为到达两个法布里-珀罗干涉仪的电场强度大小; $R_i (i=1, 2, 3, 4)$ 为反射镜面 $M_i (i=1, 2, 3, 4)$ 的反射率; α_1, α_2 分别为光在传感腔和参考腔中往返产生的总损耗。因为 $M_i (i=1, 2, 3, 4)$ 两边的介质几乎都可以看作是“空气-玻璃”,所以 R_i 可以统一用 R 来

收稿日期: 2022-07-29; 修回日期: 2022-09-08; 录用日期: 2022-09-28; 网络首发日期: 2022-10-07

基金项目: 瞬态光学与光子技术国家重点实验室开放研究基金(SKLST202105)、武汉工程大学科学基金(22QD01)

通信作者: *Wushun_wit@163.com

表示。此时,反射电场可以简化为

$$E_r = E_0 [A + B \exp(-j\phi_1) + C \sqrt{R} \exp(-j\phi_2)], \quad (2)$$

式中: $A = 2\sqrt{R}$; $B = (1 - \alpha_1)(1 - R)\sqrt{R}$; $C = (1 - \alpha_2)(1 - R)\sqrt{R}$ 。

因此,最终干涉形成的反射光强可以表示为

$$I_r \propto \left| \frac{E_r}{E_0} \right|^2 = D + I_1 + I_2 + I_3, \quad (3)$$

式中: $D = A^2 + B^2 + C^2$; $I_1 = 2AB \cos \phi_1$; $I_2 = 2AC \times \cos \phi_2$; $I_3 = 2BC \cos(\phi_1 - \phi_2)$ 。

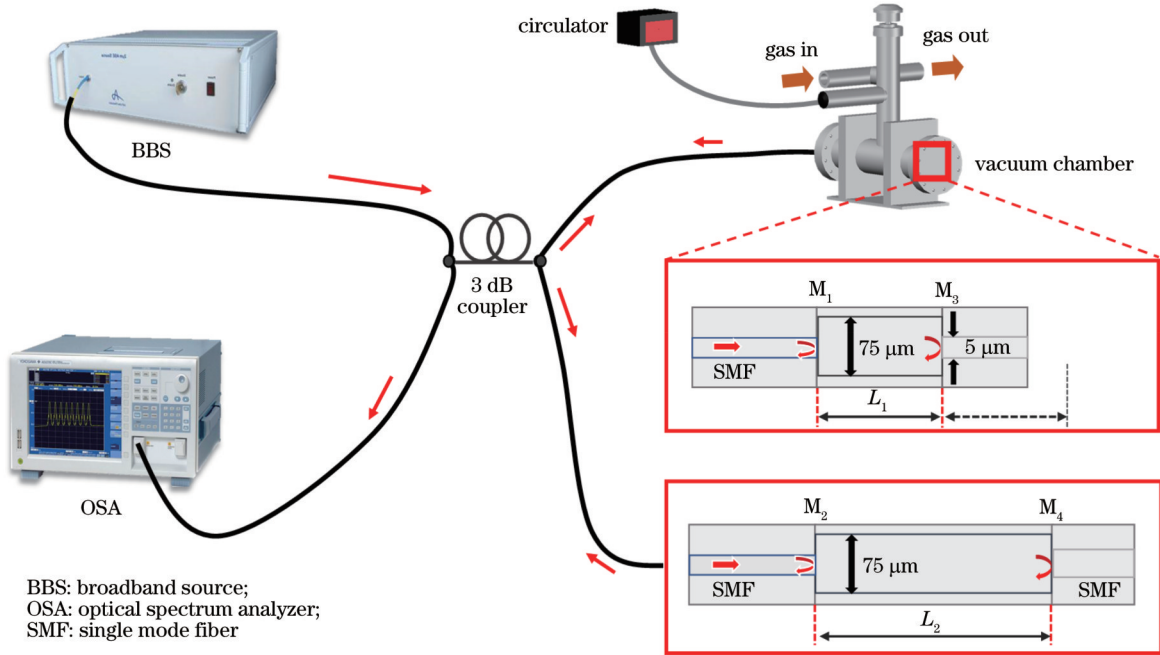


图 1 气压传感装置示意图

Fig. 1 Schematic diagram of gas pressure sensing device

通过式(3)进行模拟,可得: I_1 、 I_2 能直接决定游标光谱的主体特征,两者叠加可决定包络的基本形状; I_3 只会在此基础上增大游标包络的单边对比度。依据实验经验和文献[13, 20-21, 28],取反射率为 $R=0.04$ 、波长 λ 的取值范围为 $1300 \sim 1600 \text{ nm}$ 、 $n_1=n_2=1$ 、 $L_1=200 \mu\text{m}$,

不同 j 值 ($j=1, 2, 3, 4$) 对应的 L_2 分别为 $210, 410, 610, 810 \mu\text{m}$, 用 I_1, I_2 叠加模拟了 $j=1$ 到 $j=4$ 对应的游标光谱,如图 2 所示。可以发现:随着 j 数值的增大,外包络的对比度会随之降低;内包络的数目会随着 $j(j>1)$ 数值的增大而增多,其数目 m 可表示为 $m=j+1$ 。

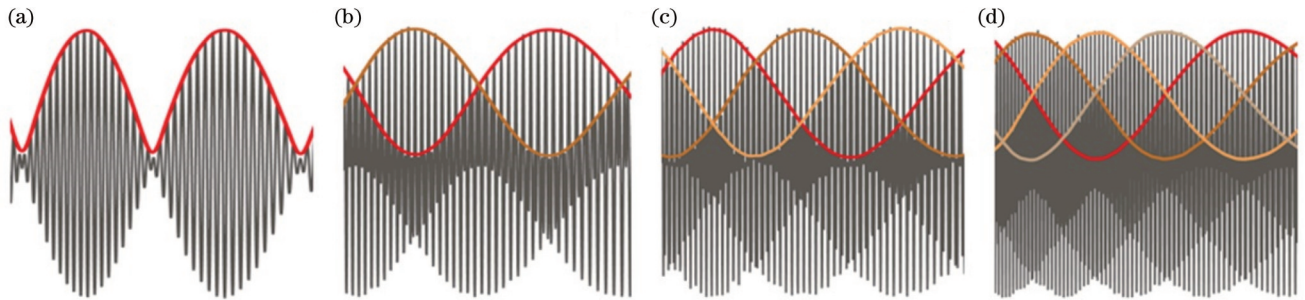


图 2 不同 j 下 I_1 和 I_2 叠加产生的光学游标光谱。(a) $j=1$; (b) $j=2$; (c) $j=3$; (d) $j=4$

Fig. 2 Optical vernier spectra produced by I_1 and I_2 superposition under different j . (a) $j=1$; (b) $j=2$; (c) $j=3$; (d) $j=4$

3 实验结果分析

本文采用图 1 所示的两个平行法布里-珀罗干涉仪结构。传感腔放置在真空腔内,它由 $75 \mu\text{m}$ 直径的空芯毛细玻璃管分别熔接单模光纤(SMF)和 $5 \mu\text{m}$ 的毛细玻璃管形成,后者作为进气口。参考腔在传感腔

的基础上将 $5 \mu\text{m}$ 空芯毛细玻璃管换成实芯的 SMF,使空气腔与外界环境隔绝,测试时放置在空气中。宽谱光源(BBS)打出的光经过 50/50 耦合器分别进入参考腔和传感腔中,然后分别依次经过 M_2-M_4 和 M_1-M_3 反射,再回到耦合器中发生干涉。干涉谱由光谱仪(O SA)显示。

在实验中,固定传感腔腔长,通过设计参考腔的腔长,制备了满足不同阶次游标效应的传感头,进而得到对应的游标光谱,如图 3 所示。当 $j < 3$ 时,实验测得的游标光谱的包络特征与理论模拟一致。当 $j = 3$ 时,仅在部分波长段内有较为清晰的包络谱。当 $j = 4$ 时,游

标包络逐渐消失。分析了不同 j 数值对应的快速傅里叶变换(FFT)图谱,发现得到的两个频率成分分别与传感腔和参考腔的腔长吻合,这表明针对不同 j 数值而设计的实验样品与游标条件对应良好。频谱图中 I_A 和 I_B 分别表示传感腔和参考腔的光强,由式(3)可知,

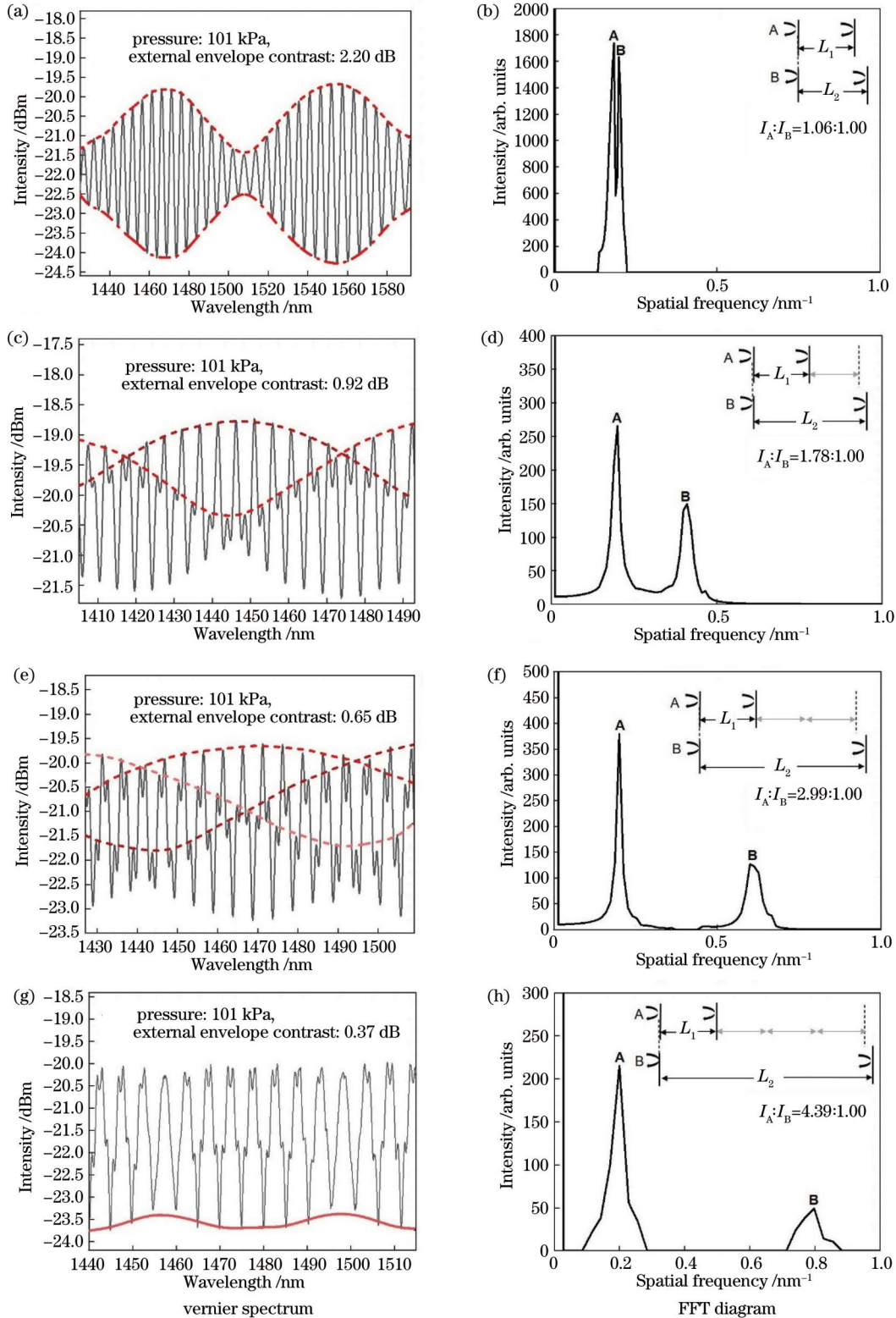


图 3 实验中不同 j 值对应的游标反射谱及其 FFT 图。(a)(b) $j=1$; (c)(d) $j=2$; (e)(f) $j=3$; (g)(h) $j=4$
 Fig. 3 Vernier spectra and FFT diagrams under different j in experiment. (a)(b) $j=1$; (c)(d) $j=2$; (e)(f) $j=3$; (g)(h) $j=4$

$I_A=2AB, I_B=2AC$, 即 I_A 和 I_B 代表了光波 I_1 和 I_2 的强度。此外,值得注意的是,随着 j 数值的增大,实验中传感腔和参考腔对应的光强比值也在增大,这与传感腔和参考腔的总损耗差异随着 j 数值的增大而增大存在一定的关系。

根据图 3 所示的结果,为了确保反射光谱能够出现清晰的游标包络特征,在测试气压灵敏度时选择

$j=2$ 的另一组样品 S1 来进行气压测试。如图 4 所示,在常温下,通过追踪内包络交叉点对应的参照点漂移情况,得出样品 S1 在 10~190 kPa 范围内对应的气压灵敏度为 152 pm/kPa,其放大倍数为 35.3,线性度为 99%。该并联结构的气压传感器相较于一般的级联结构,包络质量更佳,对恶劣环境的适应能力更强,在极端环境下的气压监测领域中具有潜在的应用价值。

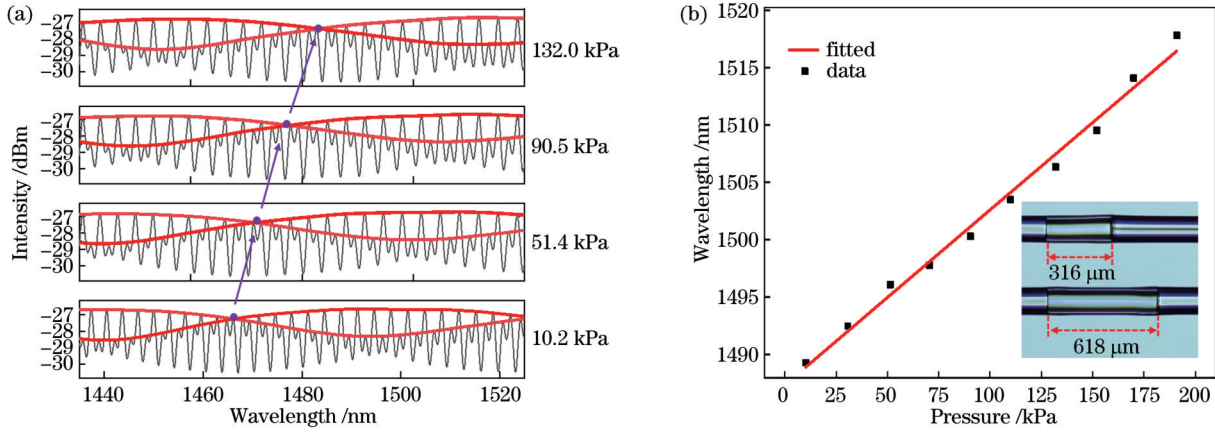


图 4 样品 S1 的气压测试结果。(a)不同气压下 S1 对应的内包络参照点漂移图;(b) S1 对应的气压灵敏度图(插图传感法布里-珀罗和参考法布里-珀罗的侧视显微图)

Fig. 4 Gas pressure test results for sample S1. (a) Drift diagram of internal envelope reference point corresponding to S1 under different air pressures; (b) gas pressure sensitivity corresponding to S1 (inset shows side-view microscopic pictures of sensing and reference Fabry-Pérot interferometers)

4 分析与讨论

为探索游标光谱的外包络对比度下降和内部包络消失的原因,依据实验中观察到的现象,从传感腔和参考腔不同的光强 (I_A 和 I_B) 比值的模拟光谱这一角度来进行讨论。维持理论部分 $j=2$ 的设定,使 ϕ_1, ϕ_2 保持不变,直接改变 I_A 和 I_B 的比值,叠加 I_1, I_2 得到如图 5 所示的光谱。当 I_A 数值不变时, I_A 与 I_B 的比值越小,对应的光学游标谱的外包络对比度越大,同时也越可能存在

内包络。这表明传感腔与参考腔的光强差异确实会影响到同一阶数对应的内包络的存在和外包络的对比度大小。结合参考文献[20],发现 j 数值增大引起的外包络对比度下降,甚至是失去基本的包络形状,也可以归因于传感腔和参考腔的光强差异过大。文献[28]中指出的条纹对比度会随着腔内光强的增大而增大的结论为此提供了相应的理论支撑,据此从包络的形成机制上进行了相关的探究。

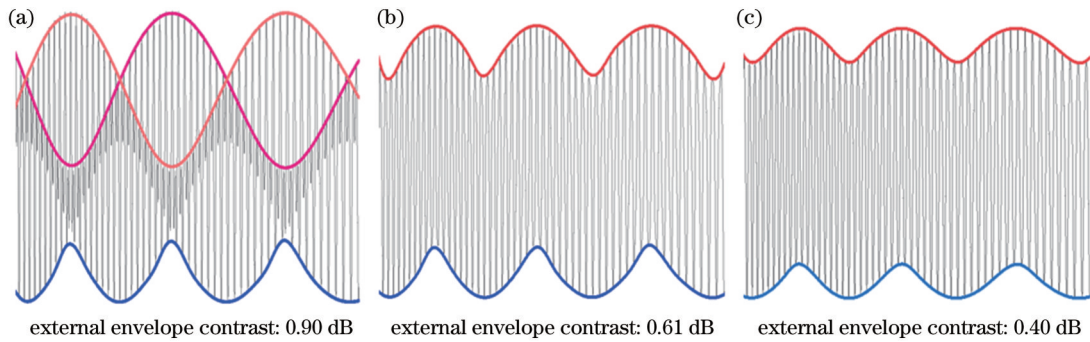


图 5 在 I_A 数值不变的情况下,不同 I_A 与 I_B 比值对应的游标光谱及其特征。(a) $I_A:I_B=2.5:1.0$;(b) $I_A:I_B=3.5:1.0$;(c) $I_A:I_B=4.5:1.0$

Fig. 5 Vernier spectra and their characteristics for different I_A to I_B ratios under constant I_A . (a) $I_A:I_B=2.5:1.0$;(b) $I_A:I_B=3.5:1.0$;(c) $I_A:I_B=4.5:1.0$

令 $\phi_1=1.0$ 、 $\phi_2=2.1$, 直接改变 I_A 与 I_B 的比值, 叠加 I_1 与 I_2 得到图 6 所示的光谱。 I_1 与 I_2 波峰叠加处会形成包络的主极大, 如图 6 中箭头所指位置所示。 I_1 、 I_2 波谷与波峰叠加的位置处会形成一个次极大, 这也是内包络的由来, 如图 6 中圆圈位置所示。当两腔光强相差较大时, 两个光波的调制效果将会减弱, 进而造成光拍的对比如度下降。当光拍对比度下降到图 6 所示的圆圈、方

框等特征点处难以辨识时, 内包络就会消失。光拍对比度减弱也意味着光谱将更容易受到光源质量或者噪声的影响, 这从根源上解释了应用高阶谐波游标效应时出现的外包络对比度低、内包络消失等光谱质量不佳的原因。综上所述, 当在传感技术中应用高阶谐波游标效应时, 应使传感腔和参考腔的光强差异尽可能减小, 这是产生完整清晰游标光谱的前提条件。

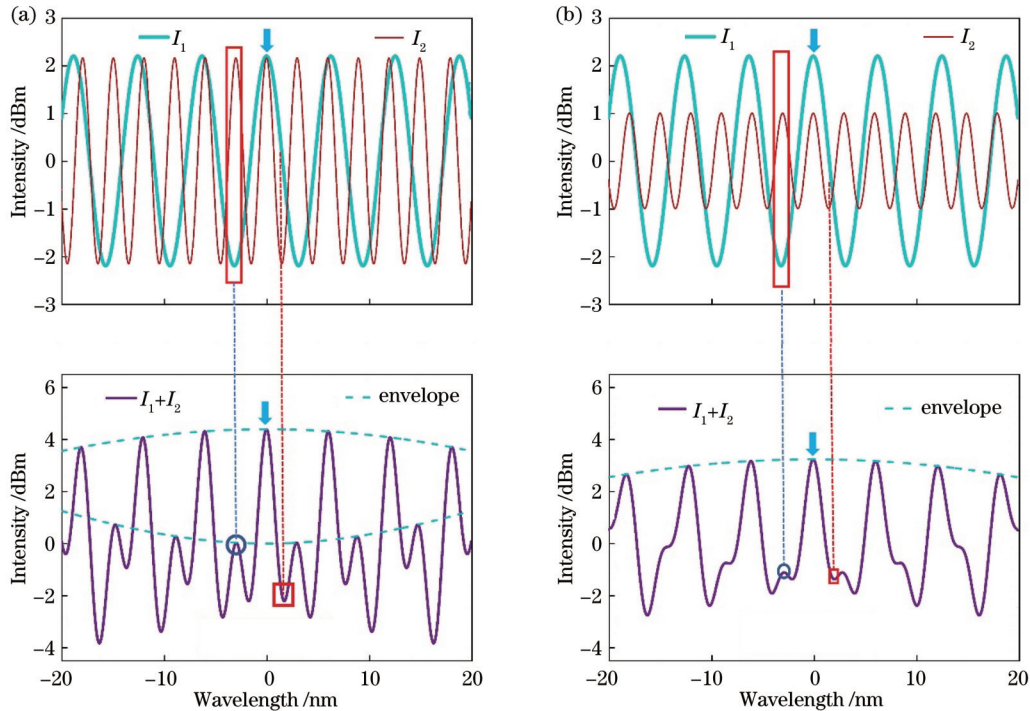


图 6 I_A 不变时 I_B 对包络特征点的影响。(a) $I_A : I_B = 1 : 1$; (b) $I_A : I_B = 3 : 1$

Fig. 6 Influence of I_B on envelope feature points under constant I_A . (a) $I_A : I_B = 1 : 1$; (b) $I_A : I_B = 3 : 1$

接着, 研究了不同参数对游标效应放大倍数的影响。由文献[20]可知, 光学游标效应的放大倍数可以表示为

$$M = \frac{M_{\text{FSR}_{\text{en}}}}{M_{\text{FSR}_2}/j} = \frac{jn_1L_1}{jn_1L_1 - n_2L_2} = \frac{jn_1L_1}{-\Delta L} \quad (4)$$

应用游标效应的主要目的就是获得更高的灵敏度。由式(4)可知, 游标放大倍数的绝对值与 j 成正比, 与失谐比 $\Delta L / (n_1L_1)$ 成反比。因此, 设计应用游标效应的传感器时的优化思路是在确保两腔光强差异不影响光谱进行数据分析的前提下, 尽可能选择更大的 j 值和更小的失谐比, 从而得到更高的游标放大倍数。合理设计传感腔的腔长、参考腔的腔长、入射光强的大小和内部损耗等系数, 以及确保腔面平整, 都是达到目标的关键。一方面, 可以通过提高阶数来获得更高的放大倍数。然而, 前文已表明, 对于高阶谐波游标效应, 传感腔和参考腔的光强差异将变大, 从而引起游标光谱对比度降低。外包络对比度低、内包络消失等游标光谱质量不佳的情况会直接影响数据分析, 故一味增大游标阶数 j 并不可取。另一方面, 增大放大倍

数也能通过增大传感腔腔长 L_1 和减小失谐量 ΔL , 以降低失谐比来实现。增大 L_1 虽然是比较常见的方法, 但是其并不适用于高阶谐波游标效应, 因为随着传感腔腔长 L_1 的增大, 参考腔腔长 L_2 也会增大, 这将引起两腔的光强差异变得更大。此外, 失谐量 $\Delta L = n_2\Delta L_2$ 与两腔的切割精度 ΔL_2 和折射率 n_2 有关。其中, ΔL_2 会受光纤切割精度限制, 折射率 n_2 可通过独特的设计来减小。在气压传感中, 由于传感腔折射率 n_1 是空气的折射率, 故即使气压改变, 其数值仍约等于 1.00。令 $L_1 = 300 \mu\text{m}$ 和 $j=1$, 图 7 显示了不同 n_2 时, 失谐比和灵敏度 $S = M \cdot S_0$ 与切割精度 ΔL_2 之间的关系, 其中 $S_0 = 4.3 \text{ pm/kPa}^{[21]}$ 。可以发现, 若参考腔介质折射率 n_2 越小, 则相同切割精度下产生的失谐量越小, 从而越有利于在相同的切割精度下得到更高的灵敏度。

5 结 论

通过理论分析和实验验证了一种基于高阶谐波游标效应的平行结构的法布里-珀罗干涉仪型光纤气压传感器。理论表明, 传感腔与参考腔反射光强差异越

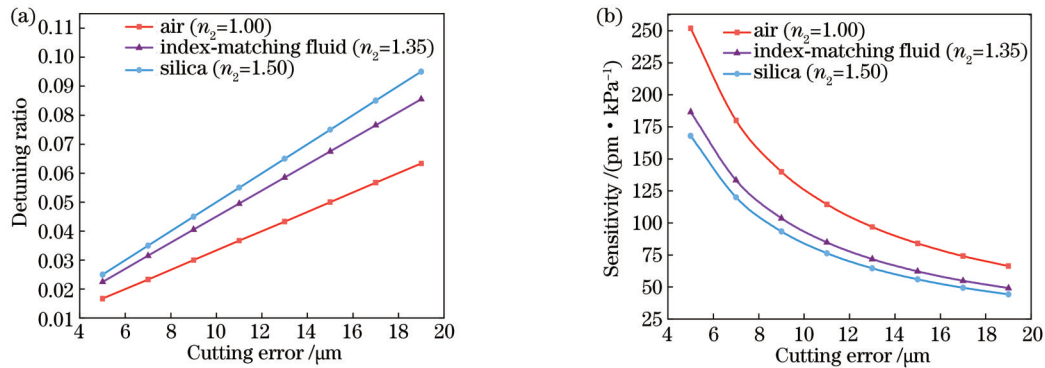


图 7 $L_1=300 \mu\text{m}$ 和 $j=1$ 时不同参考腔介质对应的切割误差与失谐比和灵敏度的关系。(a) 失谐比; (b) 灵敏度

Fig. 7 Cutting error corresponding to different reference cavity media as function of detuning ratio and sensitivity at $L_1=300 \mu\text{m}$ and $j=1$. (a) Detuning ratio; (b) sensitivity

大,产生的游标光谱的外包络对比度越小,甚至可能造成高阶谐波游标光谱的内包络消失。采用一阶谐波($j=2$)游标效应的样品 S1 进行气压测试,得到了 152 pm/kPa 的高气压灵敏度,线性度为 99% ,放大倍数可达到 35.3 ,与理论计算吻合。除此之外,还分析了如何在产生高阶光学游标效应的同时,通过合理设计传感器的参数获得高对比度的游标干涉光谱,并针对如何增大传感器灵敏度提出了合理建议。本研究为设计高灵敏度的传感器提供了思路。

参 考 文 献

- [1] Mao C, Huang B, Wang Y, et al. High-sensitivity gas pressure sensor based on hollow-core photonic bandgap fiber Mach-Zehnder interferometer[J]. Optics Express, 2018, 26(23): 30108-30115.
- [2] Wu S, Cheng H H, Ma J W, et al. Temperature-independent ultra-sensitive refractive index sensor based on hollow-core silica tubes and tapers[J]. Optics Express, 2021, 29(7): 10939-10948.
- [3] Ma J W, Wu S, Cheng H H, et al. Sensitivity-enhanced temperature sensor based on encapsulated S-taper fiber Modal interferometer[J]. Optics & Laser Technology, 2021, 139: 106933.
- [4] Gomes A D, Bartelt H, Frazão O. Optical vernier effect: recent advances and developments[J]. Laser & Photonics Reviews, 2021, 15(7): 2000588.
- [5] Quan M R, Tian J J, Yao Y. Ultra-high sensitivity Fabry-Perot interferometer gas refractive index fiber sensor based on photonic crystal fiber and vernier effect[J]. Optics Letters, 2015, 40(21): 4891-4894.
- [6] Liao H, Lu P, Fu X, et al. Sensitivity amplification of fiber-optic in-line Mach-Zehnder interferometer sensors with modified vernier-effect[J]. Optics Express, 2017, 25(22): 26898-26909.
- [7] Luo P F, Zhang M, Ghassemloooy Z, et al. Experimental demonstration of RGB LED-based optical camera communications[J]. IEEE Photonics Journal, 2015, 7(5): 7904212.
- [8] Kong L X, Zhang Y X, Zhang W G, et al. Cylinder-type fiber-optic Vernier probe based on cascaded Fabry-Perot interferometers with a controlled FSR ratio[J]. Applied Optics, 2018, 57(18): 5043-5047.
- [9] Su H Y, Zhang Y D, Zhao Y P, et al. Parallel double-FPIs temperature sensor based on suspended-core microstructured optical fiber[J]. IEEE Photonics Technology Letters, 2019, 31(24): 1905-1908.
- [10] Tian J J, Li Z G, Sun Y X, et al. High-sensitivity fiber-optic strain sensor based on the vernier effect and separated Fabry-Perot interferometers[J]. Journal of Lightwave Technology, 2019, 37(21): 5609-5618.
- [11] Wu Y, Xia L, Li W, et al. Highly sensitive Fabry-Perot demodulation based on coarse wavelength sampling and vernier effect[J]. IEEE Photonics Technology Letters, 2019, 31(6): 487-490.
- [12] Xie M Y, Gong H P, Zhang J, et al. Vernier effect of two cascaded in-fiber Mach-Zehnder interferometers based on a spherical-shaped structure[J]. Applied Optics, 2019, 58(23): 6204-6210.
- [13] Yang Y Q, Wang Y G, Jiang J X, et al. High-sensitive all-fiber fabry-perot interferometer gas refractive index sensor based on lateral offset splicing and vernier effect[J]. Optik, 2019, 196: 163181.
- [14] Li Z, Zhang Y X, Zhang W G, et al. High-sensitivity gas pressure Fabry-Perot fiber probe with micro-channel based on vernier effect[J]. Journal of Lightwave Technology, 2019, 37(14): 3444-3451.
- [15] Lin H F, Liu F F, Guo H Y, et al. Ultra-highly sensitive gas pressure sensor based on dual side-hole fiber interferometers with vernier effect[J]. Optics Express, 2018, 26(22): 28763-28772.
- [16] 刘福祿, 张钰民, 庄炜, 等. 基于游标效应和基底增敏的复合光纤结构温度传感器[J]. 光学学报, 2021, 41(15): 1506002.
- [17] Liu F L, Zhang Y M, Zhuang W, et al. Fiber temperature sensor with composite structure based on vernier effect and substrate sensitization[J]. Acta Optica Sinica, 2021, 41(15): 1506002.
- [17] 方莎莎, 吴许强, 张刚, 等. 基于游标效应的高灵敏光纤温度和应变传感器[J]. 中国激光, 2021, 48(1): 0106004.
- [17] Fang S S, Wu X Q, Zhang G, et al. High-sensitivity fiber optic temperature and strain sensors based on the vernier effect[J]. Chinese Journal of Lasers, 2021, 48(1): 0106004.
- [18] 蔡礼邹, 覃亚丽, 蔡小磊, 等. 基于游标原理的法布里-珀罗温度传感器的增敏方法[J]. 激光与光电子学进展, 2021, 58(11): 1106004.
- [18] Cai L Z, Qin Y L, Cai X L, et al. Sensitization method of Fabry-Perot temperature sensor based on vernier principle[J]. Laser & Optoelectronics Progress, 2021, 58(11): 1106004.
- [19] 郝晋青, 韩丙辰. 基于游标效应的高灵敏度光纤耦合器折射率传感器[J]. 光学学报, 2020, 40(2): 0206002.
- [19] Hao J Q, Han B C. Ultrasensitive refractive index sensor based on optical fiber couplers assisted with vernier effect[J]. Acta Optica Sinica, 2020, 40(2): 0206002.
- [20] Gomes A D, Ferreira M S, Bierlich J, et al. Optical harmonic vernier effect: a new tool for high performance interferometric

- fibre sensors[J]. *Sensors*, 2019, 19(24): 5431.
- [21] Yang X M, Wu S, Cheng H H, et al. Simplified highly-sensitive gas pressure sensor based on harmonic Vernier effect [J]. *Optics and Laser Technology*, 2021, 140: 107007.
- [22] Chen P, Dai Y T, Zhang D S, et al. Cascaded-cavity Fabry-Perot interferometric gas pressure sensor based on vernier effect [J]. *Sensors*, 2018, 18(11): 3677.
- [23] Zhang G, Wu X Q, Zhang W J, et al. High temperature vernier probe utilizing photonic crystal fiber-based Fabry-Perot interferometers[J]. *Optics Express*, 2019, 27(26): 37308-37317.
- [24] Ni W J, Lu P, Fu X, et al. Simultaneous implementation of enhanced resolution and large dynamic range for fiber temperature sensing based on different optical transmission mechanisms[J]. *Optics Express*, 2018, 26(14): 18341-18350.
- [25] Zhang P, Tang M, Gao F, et al. Cascaded fiber-optic Fabry-Perot interferometers with vernier effect for highly sensitive measurement of axial strain and magnetic field[J]. *Optics Express*, 2014, 22(16): 19581-19588.
- [26] Robalinho P, Gomes A, Frazão O. Colossal enhancement of strain sensitivity using the push-pull deformation method[J]. *IEEE Sensors Journal*, 2021, 21(4): 4623-4627.
- [27] Gomes A D, Kobelke J, Bierlich J, et al. Giant refractometric sensitivity by combining extreme optical Vernier effect and modal interference[J]. *Scientific Reports*, 2020, 10(1): 19313.
- [28] Yang X M, Li Y Q, Zhang S Y, et al. Comparison of fiber-based gas pressure sensors using hollow-core photonic crystal fibers[J]. *IEEE Photonics Journal*, 2021, 13(2): 3059925.

Analysis of Sensing Characteristics of Parallel Fabry-Pérot Interferometer Based on Vernier Effect

Luo Chunhui¹, Chen Xiaoxu¹, Wu Shun^{1,2*}

¹Hubei Key Laboratory of Optical information and Pattern Recognition, Wuhan Institute of Technology, Wuhan 430205, Hubei, China;

²State Key Laboratory of Transient Optics and Photonics, Xi'an Institute of Optics and Precision Mechanics, Chinese Academy of Sciences, Xi'an 710119, Shaanxi, China

Abstract

Objective Optical fiber sensor technology has been extensively applied in gas pressure sensing in the field of industrial and environmental safety monitoring on account of its high sensitivity, compact structure, and immunity to electromagnetic interference. Compared with long-period fiber gratings and anti-resonance waveguides, optical fiber sensors based on the vernier effect generally have greater advantages in terms of sensitivity. The vernier effect is an effective method for amplifying interferometer sensitivity, which is well-known in optical fiber sensing. However, as the harmonic order j increases, vernier spectra deteriorate, namely that the contrast of the external envelope decreases, and the inner envelope disappears. The objective of this work is to generalize the higher-order vernier effect and obtain high sensitivity through experimental exploration and theoretical analysis. In addition, we intend to explore the reasons for the decrease in external envelope contrast and the loss of internal envelopes that affect spectral contrast. We expect to contribute to the extensive application of the high-order harmonic vernier effect and high-sensitivity sensor design.

Methods Firstly, we theoretically simulate the higher-order vernier spectrum for $j=1, 2, 3, 4$. Then, we fabricate four parallel structures of the Fabry-Pérot interferometers experimentally and study the corresponding vernier spectra. After that, we investigate the effect of the difference in light intensity between the sensing cavity and the reference cavity on the vernier spectrum by changing the light intensity difference between the two cavities. In addition, we analyze various parameters that affect the vernier magnification factor and design a highly sensitive fiber-based gas pressure sensor.

Results and Discussions On the basis of a parallel Fabry-Pérot interferometer, this paper compares the theoretical simulations (Fig. 2) and the experimental results (Fig. 3) of vernier spectra for $j=1, 2, 3, 4$. The comparison shows that they are consistent, which indicates the vernier effect is valid in the experiment. After that, we simulate the spectra corresponding to different light intensities of the sensing cavity and the reference cavity. It is found that with the increase in the light intensity difference between the two cavities, the contrast of the external envelope decreases, and the internal envelope disappears (Fig. 5). Then, we fundamentally explain the deterioration of the vernier spectrum when the higher-order harmonic vernier effect is applied in the experiment (Fig. 6). In addition, the factors affecting the vernier magnification are discussed from the aspects of a higher value of j and a lower detuning ratio. After that, we put forward reasonable suggestions for obtaining higher magnification when applying the vernier effect in gas pressure sensing. Furthermore, a sample corresponding to the first-order harmonic vernier effect is produced for the gas pressure test. At room temperature, it enjoys gas pressure sensitivity of 152 pm/kPa, a corresponding magnification factor of 35.3, and

linearity of 99% in the range of 10–190 kPa (Fig. 4).

Conclusions This paper studies the higher-order harmonic vernier effect and proposes a method to improve the interference fringe contrast for the external vernier envelope, which is verified by experiments. The reason for the reduction in the vernier spectrum contrast is the reduction in the imbalance of light intensity between the sensing and the reference cavities. The application demonstrates that with the increase in the light intensity difference between the two cavities, the vernier spectrum becomes more susceptible to the quality or noise of the light source. This leads to weaker visibility of the envelope for higher harmonic orders. In addition, we analyze various experimental parameters so as to obtain high sensitivity and demonstrate a parallel Fabry-Pérot interferometer with gas pressure sensitivity of 152 pm/kPa, linearity of 99%, and a magnification factor of 35.3 in the range of 10–190 kPa.

Key words fiber optics; optical fiber sensing; gas pressure sensing; optical vernier effect; vernier spectrum